https://ntrs.nasa.gov/search.jsp?R=19670009809 2020-03-16T18:14:01+00:00Z

SELF PRESSURIZATION OF LIQUID HYDROGEN TANKAGE

A Thesis

Presented to the Faculty of the Graduate School

of Cornell University for the Degree of

Master of Science

LIBRARY COPY

JAN 3 1967

LEWIS LIBRARY, NASA
CLEVELAND, OHIO

by

John Charles Aydelott

February 1967

N67 19138 (ACCESSION NUMBER) (THRU)
64 (PAGES) 1 (CODE)
CR-82459 (NASA CR OR TMX OR AD NUMBER) 33 (CATEGORY)
FACILITY FORM 602

BIOGRAPHICAL SKETCH

The author was born February 24, 1938 in Erie, Pennsylvania, was graduated from Cornell University with a Bachelor of Mechanical Engineering in June 1961, and spent the following year at Cornell University as a teaching assistant and graduate student. Since July 1962, with the exception of two months of graduate study at Cornell University during the summer of 1964, the author has been employed by the NASA Lewis Research Center. Mr. Aydelott was the principal author of NASA publications TM X-1006 and TM X-1052 and the co-author of NASA TN D-3449.

ACKNOWLEDGMENTS

The author gratefully acknowledges the financial support of the National Aeronautics and Space Administration and the technical assistance of the Lewis Research Center personnel which made the preparation of this thesis possible.

TABLE OF CONTENTS

LIST OF TABLES

LIST OF ILLUSTRATIONS

SYMBOLS

A	surface area, sq ft
B_{jl}	absorption factor
C_p	specific heat, Btu/(lb)(^{o}R)
F	angle factor
k	thermal conductivity, Btu/(hr)(ft)(^{o}R)
L	length, ft
m	mass, lb
P	pressure, lb/sq in. abs
q	heat transfer rate, Btu/hr
Q	heat added, Btu
r	reflectivity
T	absolute temperature, ^{o}R
t	time, Hr
U	total internal energy, Btu
u	specific internal energy, Btu/lb
V	volume, cu ft
ϵ	emissivity
ρ	density, lb/cu ft
σ	Stefan-Boltzmann constant, 0.1713×10^{-8} Btu/(hr)(sq ft)(^{o}R^{4})

Subscripts:

a	absorbed

avg.	average
bulk	liquid bulk
ev	evaporation
f	final or any intermediate state
gc	gaseous conduction
i	initial state
j	summation variable
ℓ	liquid
layer	liquid thermal layer
L	at x = L
m	mean or average value
max	maximum
n	summation variable
r	radiant
s	system
sat.	saturation
sc	solid conduction
st	stored
v	vapor
w	wall
0	at x = 0
1	inner sphere
2	upper heater
3	lower heater
4	outer sphere

SUMMARY

A nonventing 9-inch-diameter spherical Dewar partially filled with liquid hydrogen was subjected to twenty-one quiescent self pressurization tests. The Dewar was subjected to various combinations of the variables percent filling, heat transfer rate, and either top heating only, bottom heating only, or uniform heating. The rate of pressure rise in the Dewar was found to be primarily a function of the heating configuration with the percent filling and heat transfer rate playing a secondary role. Appreciable energy transfer from the vapor to the liquid causing evaporation and liquid heating occurred during both the uniform heating and top heating only tests.

INTRODUCTION

The space exploration program of the National Aeronautics and Space Administration is heavily dependent on the use of liquid hydrogen as a rocket fuel. Liquid hydrogen has many properties, in addition to a very low boiling point, which set it apart from common liquids. Of particular interest are the thermal transport properties of both liquid and gaseous hydrogen which make it possible for subcooled liquid and highly superheated vapor to coexist in the same container. This situation occurs when a closed system containing liquid hydrogen is exposed to energy input in the form of heat which causes an increase in the total system pressure. The interface between the liquid and vapor phases remains at the saturation temperature corresponding to the increasing total system pressure while the average liquid temperature increases at a slower rate and thus the liquid becomes subcooled and the average vapor temperature increases at a faster rate and thus the vapor becomes superheated. As a consequence, simple thermodynamic analysis cannot predict the rate of pressure rise in a closed system containing liquid hydrogen.

An excellent review of the work that has been performed in this field will be found in (ref. 1). The majority of the reported work has been restricted to cylindrical tanks with heating only of the side walls so

that natural convection theory for vertical plates could be used to predict the heat and mass transfer within the liquid phase. In general, direct heating of the vapor was not considered.

This thesis presents the information obtained from twenty-three self pressurization tests of spherical tanks containing liquid hydrogen. The experiment consisted of a 9-inch diameter vacuum-jacketed Dewar partially filled with liquid hydrogen. The Dewar was surrounded by two hemispherical radiant heaters whose temperatures could be controlled in order to vary the distribution and rate of energy input to the hydrogen container.

Instrumentation measured Dewar pressure, vacuum-space pressure, surface temperatures of the Dewar, heater, and vacuum-jacket, and temperature at seventeen locations inside the Dewar.

Twenty-one of the tests were performed with the experiment rigidly held so that the liquid hydrogen interface was quiescent. Two tests involved violet shaking of the experiment in order to obtain a saturated homogeneous mixture of hydrogen liquid and vapor.

The purpose of the quiescent tests was to compare and explain the differences in the rate of pressure rise in a spherical hydrogen Dewar as a function of heat transfer rate, heat flux distribution, and precent filling of the container. The homogeneous tests were used for calibration of the temperature transducers and error analysis.

The experimental tests were performed at the NASA Lewis Research Center, Cleveland, Ohio during the time period from January 1965 to April 1965.

ANALYSIS

The first law of thermodynamics is

$$Q = \Delta U + P \Delta V$$

For a closed, nonexpanding system, all the heat absorbed by the system manifests itself in a change in the total internal energy of the system since $\Delta V = 0$

$$Q = \Delta U$$

If the system in question is a tank containing a liquid and its vapor, a knowledge of how the added heat affects the internal energy distribution, and thus the temperature distribution within the tank, makes prediction of the total system pressure possible. For a two-phase mixture, temperature and pressure are dependent variables at the interface between the liquid and the vapor.

The temperature distribution in a cryogenic storage tank is highly complex and is affected by many variables, the most important of which are tank geometry, percent filling, heat flux rate, and heat flux distribution.

This thesis presents two simple models that are not intended to be attempts at describing the process that actually takes place in a nonventing Dewar but are intended to be a means of comparing one set of experimental data with another. The position that experimental data

assumes in relation to the theoretical models on a plot of Dewar pressure against heat added is then an indication of how the energy is being distributed within the Dewar. Figure 1 is a plot of tank pressure as a function of heat added for two energy distribution models. The plot is for a one cubic foot container and initial fillings of 25, 50, and 75 percent. The reader may approximate the energy input, as determined by these models, that will cause a specified change in pressure for any tank size or filling. This is possible by interpolating to determine the effect of percent filling and by multiplying the heat added obtained by the volume of the tank in cubic feet since the energy input is a linear function of the tank volume. Appendix A contains the development of the first law of thermodynamics that makes the calculations for the theoretical models possible. The first model assumes homogeneous conditions throughout the Dewar and is a common calculation that is performed to compare data of this type. The second model assumes that all the energy absorbed by the Dewar goes into the evaporation of liquid. The vapor-phase temperature is always equal to the saturation temperature, which corresponds to sphere pressure. The liquid-phase temperature remains constant at the saturation temperature corresponding to seal-off pressure.

In order to obtain the energy input to a real tank a heat transfer analysis must be performed. Appendix B contains the details of the heat transfer analysis used for this experimental program. The main source of energy input to the experiment was radiant exchange from the heaters. Conduction along the plastic support ring, vent tube, and instrumentation wires played a secondary role.

Once the total energy input to the liquid hydrogen tank is known it is of interest to know how the energy input effects the contents of the tank; namely how much of the total energy input goes into heating the vapor, evaporation of liquid, or heating the liquid. At any time during the test the temperature distribution in the vapor and the pressure can be determined from the instrumentation. This makes it possible for the internal energy and mass of the vapor to be calculated at any time and thus the energy which went into heating vapor and evaporation, mass change times heat of vaporization, during the time interval of interest can be determined. The energy input to the liquid during the same time interval can then be found by subtracting the energy which went into the vapor and evaporization from the total input during the time period. From knowledge of the change in the temperature of the bulk of the liquid and the fact that the interface between the liquid and the vapor remains at the saturation temperature the energy input to the liquid can be further broken down into the energy that goes into heating the bulk of the liquid and that which heats the layer of fluid between the bulk and the liquid-vapor interface. A detailed development of this analysis will be found in Appendix C.

APPARATUS

Figure 2 is a cross-sectional drawing of the liquid hydrogen experiment that consisted of three concentric spheres; the inner sphere contained the liquid hydrogen, the intermediate sphere had electric heating coils mounted on its exterior surface, and the outer sphere served as a vacuum jacket and had coils mounted on its exterior surface through which liquid nitrogen was circulated during each test in order to minimize the conduction heat transfer to the inner sphere. The inner sphere and the heaters were painted black in order to increase their emissivity. The vent tube was made of stainless steel. The inner sphere was supported by a polychlorotrifluoroethylene plastic ring that was cut out where possible to reduce heat conduction.

A heater controller, which basically consisted of a bridge circuit which balanced the resistance of a temperature sensor on each heater with a corresponding reostat on the control panel, was used to maintain heater temperatures of 360°, 425°, 500° or 575° R.

Figure 3 shows the location of the temperature transducers on the inner sphere and the four carbon resistor temperature rakes that were located within the inner sphere to measure the temperature of the hydrogen liquid and vapor. At any time prior to a test run the resistance of any temperature transducer could be determined by the use of a digital

ohmmeter mounted in the control panel. During a test the resistance of each transducer was measured by using two bridges and amplifiers so that temperature changes were converted to 0 to 5 volt signals which were recorded on magnetic tape. For each transducer one bridge had a 0 to 5 volt range corresponding to anticipated changes in liquid temperature and the second bridge had a 0 to 5 volt range corresponding to the much larger anticipated changes in vapor temperature.

When a relatively high current is applied to a carbon resistor, its temperature is quite different depending on whether the temperature probe is in the liquid or vapor phase. This is due to self heating. Exploitation of this fact, together with careful arrangement of the carbon resistors, makes it possible to use the carbon resistors to determine the liquid level in the sphere.

Temperature transducers were located on the intermediate and outer spheres in order that the heat transfer to the inner sphere by radiation and conduction could be calculated. A single bridge recording system similar to the one used for the inner sphere temperature transducers was employed.

An ionization gage was used to measure the pressure in the vacuum space. The location of the gage and two pressure transducers used to measure the pressure in the inner sphere can be seen in figure 2. A twenty-eight volt DC power supply was used to operate the pressure transducers. The vacuum pressure was monitored continuously on the control panel. During a test the 0 to 5 volt output of the inner sphere pressure transducers was recorded on magnetic tapes.

PROCEDURE

Prior to the assembly of the experiment, thermocouples were attached to the inner sphere, heaters, and vacuum jacket. All temperature transducers were calibrated at 139.5° R by submerging the three spheres in a liquid nitrogen bath. The inner sphere, heaters, and vacuum jacket were calibrated in a carefully controlled oven at 540° R. In addition, the heater temperature transducers were calibrated at 710° R in the oven. After the experiment had been assembled it was filled with liquid hydrogen and the inner sphere temperature transducers were calibrated by violently rocking the experiment in a shaker and recording the resistance of each transducer, which corresponds to the saturation temperature of hydrogen at atmospheric pressure. Each bridge was calibrated by using a decade box to obtain a voltage versus resistance plot. Prior to each test, the pressure transducers were calibrated with standard pressure gages. Each of the calibration curves for the temperature and pressure transducers and for the bridges was curve fitted using a digital computer. The magnetic data tape from each test could then be fed into the digital computer along with the calibration curve fits and an automatic data reduction program returned printed temperature and pressure data at half second intervals for every transducer.

For each of the tests, the experiment was prepared in an identical manner; only the actual test conditions were varied. The space between the inner and outer spheres was evacuated by first using a mechanical pump and then a diffusion pump. The experiment was cooled by circulating liquid nitrogen through the coils on the outer sphere. Then the inner Dewar was filled with liquid hydrogen. The liquid nitrogen cooling and the addition of the liquid hydrogen reduced the pressure in the space between the inner and outer spheres due to cryogenic pumping. A gas meter installed in the vent line together with the carbon resistors described in the instrumentation section of this report, made it possible to determine the liquid level at the beginning of the test. The resistors accurately determine the liquid position at some time prior to the beginning of the test. The gas meter records the volume of vapor which then leaves the Dewar. Measurements of the vapor temperature, at the gas meter, and the atmospheric pressure determine the density of the vapor and the mass which leaves the Dewar before the test begins can be calculated.

The heater controller was set to maintain the desired heater temperature. All of the temperature instrumentation was checked using the digital ohmmeter and the recording system was turned on. At -1 minute the system began recording the data on magnetic tape, at zero time the vent valve was closed, and the experiment was allowed to self pressurize until a pressure of slightly over one-hundred pounds per square inch absolute was achieved. The vent valve was then opened and the pressure was allowed to decay slowly. If a sufficient amount of liquid hydrogen still remained in the experiment, a similar test at a

lower filling was run as soon as the new liquid level had been determined.

For the twenty-one quiescent tests, the experiment was mounted in a stand which was supported directly from the ground and was unattached to the surrounding structure. This permitted the experiment to remain totally undisturbed throughout the test. For the homogeneous tests, the experiment was rocked violently in a shaker so that the contents of the inner sphere stayed thoroughly mixed.

EXPERIMENTAL RESULTS

Figures 4 through 10, pressure and temperature as a function of time, present the data obtained from seven of the quiescent test runs. Each of the figures is made up of four plots; (a) total pressure as a function of time, (b) outer sphere and heater temperature as a function of time, (c) upper inner sphere temperature as a function of time, and (d) lower inner sphere temperature as a function of time. These seven tests were chosen as being representative of the twenty-one quiescent tests. Figures 4, 5, and 6 show the effect of three different percent fillings, 34.9%, 48.9%, and 76.5%, for the uniformly heated and nearly constant heat flux situation. Figures 8, 9, and 10 show the effect of three different average heat fluxs, 17.1 Btu/hr-ft^2, 27.6 Btu/hr-ft^2, and 38.2 Btu/hr-ft^2, for an approximately half full sphere which was heated only from the top. Figures 5, 7, and 9 show the effect of three different heating configurations, uniform, bottom only, and top only, for an approximately half full sphere. The bottom heating only test (fig. 7) had the same heat transfer rate from the bottom heater as the bottom heater of the uniform heating test (fig. 5). The top heating only test (fig. 9) had the same heat transfer rate from the top heater as the top heater of the uniform heating test (fig. 5). The twenty-one quiescent

tests consisted of eight tests with uniform heating, six tests with bottom heating only, and seven tests with top heating only. One of the homogeneous tests was uniformly heated and the other heated only from the top. Initial percent fillings of 35, 50, and 80 percent were desired. The high fillings proved to be the most difficult to achieve since the boil-off was too great during the period of time required to check the experiment prior to a test. Heater temperatures of approximately 360°, 500°, 575° R were used for the uniform heating tests, 500° and 575° R for the bottom heating only tests, and 425°, 500°, and 575° for the top heating only tests.

DISCUSSION OF EXPERIMENTAL RESULTS

A first look at the data would tend to suggest to the reader that the rate of pressure rise would be the most important parameter to consider when examining a group of tests which had identical heater temperatures. However, because the hydrogen vapor does become superheated and the top of the inner sphere does increase in temperature as a test proceeds this approach can be quite misleading. The heating of the inner sphere causes a reduction in the heat transfer to the hydrogen due both to the reduction in radiant exchange and the energy which is required to increase the temperature of the container wall. Higher heater temperatures and lower percent liquid fillings cause increasing inner sphere temperatures so that the average heat flux to the hydrogen is not a function only of heater temperature. As a result a better procedure is to compare the amount of heat that must be added to the Dewar to cause a given pressure rise for a particular set of conditions.

For all the tests it was assumed that the temperature profiles were symmetric with respect to the vertical axis. In other words, at any time during a test all vertical planes passing through the center of the sphere would exhibit identical temperature patterns and the left side of such a plane would be a mirror image of the right side. This assumption is based on the fact that the inner sphere, heaters, vent

tube, plastic support ring, instrumentation wires, and liquid-vapor interface all have the same symmetry with respect to the vertical axis and consequently there is no reason to anticipate that the temperature profiles would be different on opposite sides of the container. Based upon this assumption the amount of energy reradiated by the inner sphere can be calculated. The method of calculating the net radiant heat transfer and the conduction heat transfer is given in Appendix B. Heat is added to the inner sphere by radiation from the heaters, by solid conduction through the vent tube, the plastic support ring, and the temperature transducer wires, and by gaseous conduction. Figure 11 is a plot of the rate of heat input as a function of time for each of the heat sources for a typical quiescent test. The gaseous conduction of heat was negligible for all the tests. The increasing temperature of the inner sphere accounts for the reduction in the radiant heat exchange from the upper heater, as time increases, due to the increasing reradiation from the inner sphere. The increasing temperature of the inner sphere also accounts for the decreasing and eventually negative conduction heat transfer from the vent tube since the inner sphere becomes hotter than the liquid nitrogen cooled outer sphere and heat is conducted away from the top of the inner sphere

Table I is a summary of the experimental results and the heat transfer analysis. The initial percent filling was determined as explained in the PROCEDURE section. The pressure rise rate is an average value obtained by dividing the difference between the pressure at the end of the test and atmospheric pressure in psia by the total test time. The bulk temperature was taken to be the lowest recorded

temperature, usually temperature transducers 11 or 12. Dividing the change in the bulk temperature, during the test, by the change in the saturation temperature during the test, gives an indication of how much energy went into heating the liquid and thus how nearly homogeneous the liquid is at the end of the test. The maximum change in the vapor temperature gives an indication of how much energy went into superheating the the vapor. The average heat flux is determined by dividing the total energy input to the hydrogen as determined in Appendix B by the test time and the surface area of the inner sphere. This average is then broken down into the heat flux through the liquid wetted walls and through the walls exposed to vapor. Breaking the heat flux up into parts in this manner clearly shows the effect of the increasing upper inner sphere temperature which reduces the net radiant heat exchange.

The two homogeneous tests were run for the purpose of checking the validity of the heat transfer analysis and to get an estimate of the accuracy of the instrumentation. Figure 12 is a plot of sphere pressure as a function of heat added for the two homogeneous tests. One test was run with only the top heater installed, the other with both heaters installed. For both tests the experiment was shaken vigorously so that the hydrogen liquid and vapor were thoroughly mixed and at the saturation temperature corresponding to the absolute inner sphere pressure. Since the initial filling and pressure were known, a theoretical plot of homogeneous pressure versus heat added, shown as dashed lines on figure 12, was generated using the analytical technique presented in Appendix A. Every thirty seconds the test data was used to perform a heat transfer analysis, as presented in Appendix B, and

the heat added up to that point in time was plotted aginst the experimentally recorded pressure. These calculated points are identified by the symbols on figure 12. By superimposing the data obtained from the heat transfer analysis on the theoretical homogeneous line the combined experimental and analytical error can be seen. Ideally the calculated points should fall on the theoretical line, but a maximum error of two pounds per square inch or two percent of full scale was observed.

The homogeneous tests also provided a check on the accuracy of the inner sphere temperature transducers since saturation temperature should be recorded during the entire test. As in the previous discussion where it was impossible to separate the error associated with the pressure transducer from the error in the heat transfer analysis; here it will be impossible to separate the error associated with the pressure transducer from the error associated with the temperature transducers. If it is first assumed that the pressure transducer is correct, the carbon resistor temperature transducers indicate saturated conditions within a maximum of $\pm 0.6^{\circ}$ R with an average error of -0.3° R in the range from 36 to 54° R. The platinum surface temperature transducers indicate saturated conditions within a maximum of $+2.2^{\circ}$ R with an average error of $+0.9^{\circ}$ R. Figure 13 is a plot of resistance as a function of temperature for typical inner sphere temperature transducers. This figure shows that in the temperature range of 36 to 54° R the carbon resistors under go approximately a seventy ohm change in resistance while the platinum surface transducer resistance only changes four ohms for each degree Rankine change in temperature.

Consequently, at these low temperatures it would be expected that the carbon resistor temperature transducers would be more accurate. If it is now assumed that the carbon resistors are indicating the true saturation conditions, then the pressure transducer would have a maximum error of two pounds per square inch, or the same result obtained from the discussion associated with figure 12. Figure 13 is also useful in estimating the accuracy of the temperature transducers at higher temperatures. In the 200^{O} to 300^{O} R range the carbon resistance transducers under go approximately a two ohm change in resistance for each Rankine degree as compared to a seventy ohm change for each Rankine degree at the lower temperatures. This indicates that the resistors are less accurate by a factor of thirty-five at the higher temperatures so that errors as high as $\pm 20^{O}$ R may be possible. Above 100^{O} R the platinum surface transducer resistance changed seven ohms for each degree Rankine change in temperature so that these transducers should be slightly more accurate at higher temperatures than in the liquid hydrogen temperature range. In summary, because both the heat transfer analysis and the carbon resistors temperature transducers indicated the same error in the pressure transducers, it is reasonable to assume that the pressure data is accurate within two pounds per square inch, the platinum surface temperature transducers are accurate within two degrees Rankine, and the carbon resistor temperature transducers are accurate to three-tenths of a degree Rankine at low temperatures and ten degrees Rankine at high temperatures.

Figure 14a shows the effect of heat transfer rate and distribution on the sphere pressure as a function of total heat added for the approxi-

mately fifty percent filled quiescent tests. The fifty percent filled tests were chosen since they represent the least complicated geometric situation where the liquid-vapor interface and the division between the upper and lower heaters are approximately in the same horizontal plane. It is readily apparent that the heating configuration is the primary factor affecting the slope of the pressure versus heat added data. The heat transfer rate had the least effect on the slope of the pressure versus heat added data for the bottom heated tests with increasing influence on the uniformly heated and top heated tests. However, the heat transfer rate was definitely secondary in importance to the heating configuration. Since the two coordinates, pressure and heat added, are the integrals over time of pressure rise rate and heat transfer rate, coincident test data indicates a linear relationship between pressure rise rate and heat transfer rate; that is, doubling the heat rransfer rate will double the pressure rise rate. For the bottom heated tests this linear relationship was followed almost exactly, but the uniformly heated tests, and to a greater degree, the top heating only tests began to deviate. This indicates that the way in which energy was distributed in the liquid was unaffected by the rate of energy input, while the rate of energy input to the vapor greatly affected the resulting temperature or energy distribution. Analysis based on the Rayleigh number indicates that the mode of heat transfer in the liquid would be turbulent convection (ref. 2). However, a summary of liquid hydrogen boiling studies presented in reference 3 indicates that at the heat fluxs employed for these tests boiling is quite likely to occur. An essentially uniform temperature liquid bulk would be anticipated for either turbulent

convection or boiling heat transfer. Because a uniform temperature liquid bulk was experimentally observed, it is reasonable to assume that at the lower heat fluxs the heat transfer mechanism in the liquid was dominated by turbulent convection with some boiling entering in at the higher heat fluxs. The heat transfer processes which take place in the vapor are not clearly understood, but additional discussion will be presented after the energy distribution analysis, Appendix C, is introduced. The theoretical surface evaporation and homogeneous lines which appear on figure 14a also help the reader to understand how the energy distribution within the hydrogen container effects the experimental results. It will be recalled that the surface evaporation model is based on the concept of no heating of the liquid coupled with a saturated vapor while the homogeneous model has both saturated liquid and saturated vapor at all times. The top heating only tests approach the surface evaporation model in one respect; the liquid is heated a very slight amount, but superheating of the vapor pushes the experimental data above the theoretical surface evaporation line. The bottom heating only tests approach the homogeneous model in one respect; the liquid is nearly saturated, but some heating of the vapor causes superheating and the experimental data lies above the theoretical homogeneous line. The uniformly heated tests combine some heating of the liquid with superheating of the gas with the resulting data lying between the two extremes of top and bottom heating only.

Figure 14b shows the effect of percent filling on the sphere pressure as a function of heat added for three uniformly heated tests. The data presented is for test numbers 3, 4, and 5. These three tests

were chosen to demonstrate the effect of percent filling because the average heat flux for the three tests was nearly the same. Due to the increase in temperature of the upper part of the sphere the low filling test had the lowest average heat flux. Based on the information obtained from figure 14a it would be expected that if the average heat flux had been the same the experimental data would have been somewhat closer together than that shown in figure 14b. The obvious conclusion to be drawn from figure 14b is that the rate of pressure rise was only slightly affected by varying the percent filling, with a trend toward higher rates of pressure rise at higher fillings for the uniformly heated tests. In order to understand why the rate of pressure rise is only slightly affected by the percent filling, for the uniformly heated tests, reference is again made to table I. The data for test numbers 3, 4, and 5 indicate that as the percent filling is increased the liquid becomes less subcooled and the vapor becomes less superheated. These two effects tend to counterbalance each other. In contrast, the bottom heating only tests exhibit decreasing rates of pressure rise with increasing filling, a result of the increased, nearly saturated liquid mass which is available to absorb the incoming energy. The top heating only tests exhibit increasing rates of pressure rise with increasing filling, a result of the increasing unheated liquid mass which effectively reduces the volume of the container. Evidently the uniformly heated tests are slightly dominated by the heating of the vapor which causes a small increase in the rate of pressure rise with increasing filling.

In order to further explain the experimental results an analysis was performed to determine what percentage of the incoming energy resulted in heating of the liquid bulk, the liquid thermal layer, evaporation of liquid, and superheating of the vapor. The details of these energy distribution calculations will be found in Appendix C. Figure 15 shows the inner sphere temperature as a function of position for a typical quiescent test. The liquid-vapor interface is located at a value of height to radius of 0.8. This figure shows that the temperature of the vapor space was only a function of the vertical coordinate since the data for all the instrumentation, both centrally located and near the container wall, had the same temperature profile. Consequently, the energy distribution analysis was based on the assumption that the vapor space could be divided up into horizontal uniform temperature discs. These discs, or elemental volumes, were then used to perform a summation, approximating an integration, to determine the total mass and internal energy of the vapor space at any time during the test. The total vapor internal energy is divided by the mass of vapor to determine the average vapor specific internal energy which together with the pressure defines an average vapor temperature. Knowledge of the change in internal energy and mass of the vapor as a function of time allows the calculation of the percentage of the energy input which superheated the vapor and caused evaporation. The percentage of the energy input which heated the liquid is determined by subtracting the input to the vapor and for evaporation from the total energy input calculated from the heat transfer analysis The mass of the system is a constant so the mass of the liquid can be determined at any time by

subtracting the mass of the vapor from the total initial mass. The average liquid internal energy is calculated from knowledge of the initial conditions and the energy input to the liquid. Any average property of the liquid can now be determined since the pressure and average internal energy are known at any time. The average liquid density is calculated which together with the mass of the liquid makes it possible to determine the percent filling at any time. The average percent filling is converted to an average liquid wetted area and multiplied by the wetted area heat transfer rate to determine the energy input to the liquid hydrogen. The energy input to the liquid was further broken down into two parts; the energy which went into the bulk of the liquid and the energy which went into heating the thermal layer between the saturated liquid-vapor interface and the bulk of the liquid. Figure 16 is a plot of inner sphere temperature as a function of position for three heating configurations. Of particular interest are the temperature profiles in the liquid for the three tests. It can be seen that the bulk temperature, or lowest recorded temperature, is representative of a large portion of the liquid mass. For the purposes of mathematical computation a linear temperature gradient from the bulk temperature to the saturation temperature at the interface was assumed. It is realized that for some of the tests this is a poor approximation to the actual temperature gradient, but the analysis based on this approximation helps to further explain how energy is transported and distributed within the liquid hydrogen.

Table 2 is a summary of the results of the energy distribution analysis. It will be noted that four tests were not included in the energy

distribution analysis. Geometric considerations were responsible for the exclusion of these tests. The two low filling bottom heated only tests had some direct heating of the vapor. The two high filling top heated only tests had some direct heating of the liquid. It is impossible to separate the total energy input into the quantity which heated liquid and that which heated vapor so the tests were not included.

The lower heating only tests proved to be the easiest to understand and the least interesting. The energy input to the liquid wetted walls accounted for the heating of the bulk liquid, which was nearly saturated, the energy input to a thin liquid thermal layer and the energy which went into evaporation. What heating of the vapor that did occur was due to the small energy input to the dry walls. Considering the accuracy of the instrumentation and the analysis, it is quite possible that no thermal layer existed and the experiment under the bottom heating only condition was equivalent to heating a container of water on the kitchen stove. The top heating only tests proved to be just the opposite; the hardest to understand and the most interesting. As before, the energy input to the liquid wetted walls approximately accounted for the heating of the liquid bulk, but the energy input to the dry walls heated the vapor, supplied the energy for evaporation and heated the liquid thermal layer with over fifty percent of the total energy input ending up in the liquid thermal layer. It seems reasonable to assume that the energy transfer from the vapor to the liquid was intermolecular in nature. The fact that the lines of constant temperature in the vapor were horizontal, with increasing temperature at higher vertical positions, rules out the possibility of any convective flow. It is possible

that an involved conduction analysis could predict both the vapor and the liquid thermal layer gradients; however, a detailed analysis was not undertaken. An order of magnitude type analysis using the observed temperature gradients and rates of heat transfer has indicated that conduction could be the primary mode of energy exchange. It was not felt that the experiment design, or the accuracy of the instrumentation and analysis, lent itself to further pursuit of this line of thought. The results of the analysis on the uniformly heated tests were easily identified as being the combined results of the top heating only and bottom heating only tests. The energy input to the dry walls heated the vapor, supplied the necessary energy for evaporation, and heated most of the liquid thermal layer. The energy input to the liquid wetted walls heated the liquid bulk and a portion of the liquid thermal layer. It is quite possible that the inaccuracies in the analysis would account for the portion of the heating of the liquid thermal layer which came from the liquid wetted walls. These inaccuracies come from the assumption of a linear temperature gradient in the liquid thermal layer, the fact that the energy passing through the liquid wetted walls near the interface must add to the thermal layer, and consideration of the fact that as the test proceeds the liquid thermal layer grows and liquid which was previously included in the bulk now becomes part of the thermal layer. The rate of pressure rise in the hydrogen container, for the uniformly heated tests, is primarily a function of the energy input to the vapor since the energy input to the liquid wetted walls primarily heats the liquid bulk. The only contribution which heating the liquid makes to the

container pressure is due to the thermal expansion of the liquid. Liquid hydrogen does have a relatively high coefficient of thermal expansion, but this effect is secondary to the energy input to the vapor for determining the rate of pressure rise.

To summarize the experimental results obtained from the twenty-one quiescent tests, a simple calculation was performed. The average liquid and vapor temperatures, obtained from the energy distribution analysis, together with the pressure at the beginning and end of each test were used to compute the average liquid and vapor specific entropy. Knowledge of the mass of the liquid and vapor both at the start and end of the test made it possible to determine the total change in system entropy during the test. This change in system entropy was divided by the change in entropy of the corresponding homogeneous model and the resulting dimensionless parameter was termed the homogeneity factor. Figure 17 is a plot of the homogeneity factor as a function of average heat transfer rate for the quiescent tests.

The thermodynamic property entropy is often associated with probability. It was with this thought in mind that the change in entropy of a real system, as compared to a theoretical homogeneous model, was chosen as the single parameter most suitable for summarizing the experimental results. A homogeneity factor equal to unity would be for a homogeneous system. In contrast, systems with low homogeneity factors exhibit large temperature gradients. If isolated, these systems would decay to the uniform temperature, more probable, situation found in a homogeneous system. The length of the lines on figure 17 is indicative of the range of heat flux that was explored for

each percent filling and heating configuration while the thickness of the lines represents the authors confidence limits. Nothing new or unexpected resulted from this entropy calculation. Once again, it is apparent that the heating configuration is the most important variable effecting the final state of the system. The heat transfer rate was of significant influence only on the upper heating only tests. For the lower heating only tests, the high fillings were more nearly homogeneous since the vapor mass, which was slightly superheated, was smaller. For the upper heating only tests the high fillings were less homogeneous since the mass of the liquid bulk, which essentially did not change temperature, was larger. The uniformly heated tests showed the influence of both the top and bottom heating effects with the top heating dominating the overall final system conditions.

SUMMARY OF RESULTS

A nonventing 9-inch-diameter spherical Dewar partially filled with liquid hydrogen was subjected to twenty-one quiescent self pressurization tests. The tests were terminated at a maximum pressure of one-hundred pounds per square inch absolute. The Dewar was subjected to various combinations of the variables percent filling, heat transfer rate, and either top heating only, bottom heating only, or uniform heating. The following results were obtained:

(1) The rate of pressure rise was affected most by heater configuration, being greatest for the top heating only tests, least for the bottom heating only tests.

(2) The rate of pressure rise increased almost linearly with increasing heat transfer rate.

(3) The rate of pressure rise was only slightly affected by varying the percent filling.

(4) Appreciable energy transfer from the vapor to the liquid causing evaporation and liquid heating occurred during both the uniform heating and top heating only tests.

(5) Nearly saturated liquid temperatures were recorded throughout the liquid for the bottom heating only tests.

APPENDIX A

THERMODYNAMIC CALCULATIONS

One method of analyzing a system thermodynamically is to define the conditions at the beginning and the end of a process; then the necessary input to the system can be determined. For the problem of a Dewar, which is sealed at the beginning of the test, the initial condition is that the Dewar contains a homogeneous mixture at atmospheric pressure with a known percent filling. The final condition is defined by the model being considered. For a nonexpanding closed system, the input is heat, and as stated by the first law of thermodynamics:

$$Q = \Delta U \tag{A1}$$

For the development of this analysis, the initial state will be signified by the subscript i and the final, or any intermediate state, is denoted by the subscript f. Equation (A1) may be written

$$Q = U_f - U_i = \left(m_{\ell,f}u_{\ell,f} + m_{v,f}u_{v,f}\right) - \left(m_{\ell,i}u_{\ell,i} + m_{v,i}u_{v,i}\right) \tag{A2}$$

The density and specific internal energy of each phase at state i can be found if the system is known to be homogeneous and at the saturation temperature corresponding to atmospheric pressure (ref. 4). The total internal energy at state i can then be determined since

$$m_{\ell,i} = \rho_{\ell,i} \frac{(\text{percent filling})_i}{100} V \tag{A3}$$

$$m_{v,i} = \rho_{v,i} \left[1 - \frac{(\text{percent filling})_i}{100} \right] V \tag{A4}$$

For a closed nonexpanding system, the mass of the liquid plus the mass of the vapor is a constant; consequently, the system density is a constant:

$$\rho_s = \frac{(\text{percent filling})_i}{100} \rho_{\ell,i} + \left[1 - \frac{(\text{percent filling})_i}{100} \right] \rho_{v,i} \tag{A5}$$

For the homogeneous model, state f (and thus the density and internal energy of each phase) is defined by the fact that the system is homogeneous and at the saturation temperature corresponding to the system pressure. Equation (A5), written for state f, can be solved for the percent filling at state f:

$$(\text{percent filling})_f = \frac{\rho_s - \rho_{v,f}}{\rho_{\ell,f} - \rho_{v,f}} (100) \tag{A6}$$

The total internal energy at state f can then be determined since

$$m_{\ell,f} = \rho_{\ell,f} \frac{(\text{percent filling})_f}{100} V \tag{A7}$$

and

$$m_{v,f} = \rho_{v,f} \left[1 - \frac{(\text{percent filling})_f}{100} \right] V \tag{A8}$$

The amount of heat required to reach state f for the homogeneous model can now be calculated by using equation (A2).

For the surface-evaporation model, state i is the same as that for the previous model so that the total internal energy at state i is found by the identical procedure. The surface-evaporation model is based on the concept that all of the energy goes into evaporating the liquid, so that the density and internal energy of the remaining liquid will be unaltered by the process; that is, $\rho_{\ell,i} = \rho_{\ell,f}$ and $u_{\ell,i} = u_{\ell,f}$. The density and internal energy of the vapor are defined by the fact that the vapor is homogeneous and at the saturation temperature corresponding to the final system pressure. Equation (A5), written for state f, can be solved for the percent filling at state f

$$(\text{percent filling})_f = \frac{\rho_s - \rho_{v,f}}{\rho_{\ell,i} - \rho_{v,f}} \, 100 \tag{A9}$$

The mass of liquid and vapor at state f can then be determined since

$$m_{\ell,f} = \rho_{\ell,i} \frac{(\text{percent filling})_f}{100} V \tag{A10}$$

and

$$m_{v,f} = \rho_{v,f} \left[1 - \frac{(\text{percent filling})_f}{100} \right] V \tag{A11}$$

The total internal energy at state f can now be determined, and from equation (A2), the heat required to reach state f for the surface-evaporation model can be calculated.

APPENDIX B

HEAT TRANSFER CALCULATIONS

The amount of energy absorbed by the contained hydrogen is equal to the heat transferred to the sphere by radiation, solid conduction, and gaseous conduction minus the amount of energy stored in the container itself; that is

$$Q_a = (q_r + q_{sc} + q_{gc})\,\Delta t - Q_s t \qquad \text{(B1)}$$

The amount of heat transferred by thermal radiation from the heated intermediate sphere to the inner sphere is determined by the method presented in reference 2. For the radiant exchange calculations the inner sphere is assigned the number 1, the upper heater number 2, the lower heater number 3, and the outer sphere number 4. The net rate of radiant heat absorbed by the inner sphere when both heaters are installed is

$$q_1 = \sum_{j=1}^{3} \sigma B_{j1} \epsilon_j A_j T_j^4 - \sigma \epsilon_1 A_1 T_1^4 \qquad \text{(B2)}$$

where B_{j1}, the absorption factor, is defined as the fraction of the total radiant energy emission of surface j which is absorbed by surface 1. The absorption factors are determined by solution of the following simultaneous equations:

$$(F_{11}r_1 - 1)B_{11} + F_{12}r_2B_{21} + F_{13}r_3B_{31} + F_{11}\epsilon_1 = 0 \qquad (B3)$$

$$F_{21}r_1B_{11} + (F_{22}r_2 - 1)B_{21} + F_{23}r_3B_{31} + F_{21}\epsilon_1 = 0 \qquad (B4)$$

$$F_{31}r_1B_{11} + F_{32}r_2B_{21} + (F_{33}r_3 - 1)B_{31} + F_{31}\epsilon_1 = 0 \qquad (B5)$$

This technique treats all diffuse-radiation circumstances and requires only a knowledge of the geometry of the three surfaces, the average temperature of the surfaces, and the emissivity of the surfaces as shown in figure 18. The data for this figure was obtained experimentally by Lewis Research Center personnel using a sample surface identical to those of the experiment.

When one of the hemispherical heaters was removed in order to obtain only top or bottom heating the outer sphere, surface 4, had to be substituted for the removed heater, surface 2 or 3, in equation (B2) and subsequent calculations. The inside of the outer sphere was gold plated and an emissivity of 0.10 was assumed. Due to the variation in temperature of the inner sphere the last term in equation (B2) was expressed as an integral and called the inner sphere reradiated heat flux

$$q_{1_{\text{reradiated}}} = \int_{A_1} \sigma\epsilon T^4 \, dA \qquad (B6)$$

where A_1 is the surface area of the inner sphere. This integral was approximated by the summation

$$q_{1_{\text{reradiated}}} \approx \sum_{j=1}^{n} \sigma\epsilon_j T_j^4 \, \Delta A_j \qquad (B7)$$

As explained in the **DISCUSSION OF EXPERIMENTAL RESULTS** section, the temperature of the inner sphere was found to be only a function of the

vertical coordinate so that horizontal uniform temperature sections could be used to divide the sphere into elemental surface areas. A digital computer was used to curve fit the emissivity versus temperature curve and the inner sphere temperature versus position curves for each time interval. An average temperature for each elemental area was used to determine the local emissivity and the summation was performed every thirty seconds by using a digital computer.

The energy stored in the container at any time interval was also expressed as an integral

$$Q_{s_t} = \int_{V_{1w}} C_p \rho T \, dV \tag{B8}$$

where V_{1w} is the volume of the container wall. This integral was approximated by the summation

$$Q_{s_t} \approx \sum_{j=1}^{n} \rho C_{pj} T_j \Delta V_j \tag{B9}$$

Assuming the same temperature distribution, a digital computer was used to curve fit the stainless steel specific heat as a function of temperature curve found in figure 19 (ref. 5) and the inner sphere temperature versus position curves for each time interval. An average temperature for each elemental volume was used to determine the specific heat and the summation was performed every thirty seconds by using a digital computer.

The differential equation and boundary conditions for one-dimensional heat transfer by solid conduction are the following:

$$\frac{d}{dx}\left(k\frac{dT}{dx}\right) = 0 \begin{cases} \text{at } x = 0, & T = T_0 \\ \text{at } x = L, & T = T_L \end{cases} \qquad \text{(B10)}$$

At the very low temperatures encountered with the use of liquid hydrogen, the thermal conductivity of most materials is highly temperature dependent and can be expressed as some function of the absolute temperature. Substituting the boundary conditions in equation (B10) and integrating (ref. 2) result in

$$\frac{q}{A} = k_m \frac{T_0 - T_L}{L} \qquad \text{(B11)}$$

where

$$k_m = \frac{1}{T_L - T_0} \int_{T_0}^{T_L} k(T)\, dT \qquad \text{(B12)}$$

Figure 20 shows the stainless steel thermal conductivity as a function of temperature (ref 5) and the curve fit which was used to perform the necessary ingegration in equation (B12). Figure 21 shows the plastic support ring thermal conductivity as a function of temperature and the curve fit which was used to perform the necessary integration in equation (B12). The data for this figure was obtained experimentally by Lewis Research Center personnel using a sample piece of plastic identical to that used in the experiment.

For all the tests, the heat transfer due to gaseous conduction through the vacuum space, was negligible.

APPENDIX C

ENERGY DISTRIBUTION CALCULATIONS

As explained in the DISCUSSION OF EXPERIMENTAL RESULTS section, the temperature of the hydrogen vapor was found to be only a function of the vertical coordinate so that horizontal uniform temperature sections could be used to divide the vapor space into elemental volumes. Each elemental volume then approximated a region of constant temperature and pressure. Since two thermodynamic properties are known, for each elemental volume, any other property can be determined. The properties of particular interest are the density and specific internal energy. The equations which were used to generate the hydrogen tables, reference 4 were curve fitted using a digital computer so that the desired properties were readily available once the pressure and temperature were known. This made it possible to determine the total internal energy and mass of the vapor at any time.

$$m_v = \int_{V_v} dm_v \qquad (C1)$$

$$U_v = \int_{V_v} u_v \, dm_v \qquad (C2)$$

These two integrals were approximated by the summations:

$$m_v \approx \sum_{j=1}^{n} \rho_{v_j} \Delta V_{v_j} \tag{C3}$$

$$U_v \approx \sum_{j=1}^{n} u_{v_j} \rho_{v_j} \Delta V_{v_j} \tag{C4}$$

At any time these summations can be evaluated by using a digital computer. It is first necessary to curve fit the vapor temperature versus position data for the test times of interest. The computer can then determine the necessary properties, from the hydrogen property curve fits, for each elemental volume, and perform the necessary mathematical operations. The energy input to the vapor during any time interval is

$$Q_v = U_{v_f} - U_{v_i}$$

The change in the mass of the vapor is:

$$\Delta m_v = m_{v_f} - m_{v_i} \tag{C5}$$

The energy input that results in evaporation is

$$Q_{ev} = (\Delta m_v)(\text{heat of vaporization}) \tag{C6}$$

The energy input to the liquid is determined by subtracting the energy input to the vapor and evaporation from the total energy input to the container.

$$Q_\ell = Q_1 - Q_v - Q_{ev} \tag{C7}$$

In order to further explore the energy distribution within the liquid phase it was assumed that the liquid consisted of a uniform temperature region known as the bulk and a region of linear temperature change between the bulk and the liquid-vapor interface known as the thermal

layer. This assumption is considered in detail in the DISCUSSION OF EXPERIMENTAL RESULTS section. The bulk temperature, at any time, is determined from the instrumentation and the thermal layer average temperature is:

$$T_{layer} = \frac{T_{bulk} + T_{sat.}}{2} \tag{C8}$$

Since the liquid-vapor interface is always at the saturation temperature, the average internal energy of the liquid initially corresponds to the saturated temperature and pressure and at any later time is:

$$u_{\ell_{avg.}} = u_{\ell_i} + \frac{Q_\ell}{m_\ell} \tag{C9}$$

where: $m_\ell = m_{\ell_i} - \Delta m_v$

At any time the energy stored in the liquid must be equal to the sum of the energy stored in the two regions.

$$m_\ell u_{\ell_{avg}} = m_{bulk} u_{bulk} + m_{layer}\left(\frac{u_{bulk} + u_{sat}}{2}\right) \tag{C10}$$

The total mass of liquid is equal to the sum of the mass of liquid in the two regions.

$$m_\ell = m_{bulk} + m_{layer} \tag{C11}$$

Combination of equations (C10) and (C11) yields:

$$m_{bulk} = m_\ell \frac{\left(u_{\ell_{sat}} + u_{bulk} - 2u_{\ell_{avg}}\right)}{u_{\ell_{sat}} - u_{bulk}} \tag{C12}$$

All of the liquid is initially saturated so the energy input to the bulk is:

$$Q_{bulk} = m_{bulk_f} u_{bulk_f} - m_{\ell_i} u_{\ell_{sat_i}} \tag{C13}$$

and by subtracting the energy input to the bulk from the total energy input to the liquid:

$$Q_{layer} = Q_{\ell} - Q_{bulk} \tag{C14}$$

The percent filling of the inner sphere at any time is

$$\text{percent filling} = \frac{m_{\ell}}{\rho_{\ell_{avg}} V} \times 100 \tag{C15}$$

where $\rho_{\ell_{avg}}$ is determined by using the computer and the values of the total sphere pressure and $u_{\ell_{avg}}$ as input.

BIBLIOGRAPHY

1. Clark, J. A.: A Review of Pressurization, Stratification, and Interfacial Phenomena. International Advances in Cryogenic Engineering, Proceedings of the 1964 Cryogenic Engineering Conference. pp. 259-283, Plenum Press, 1965.

2. Gebhart, Benjamin: Heat Transfer. McGraw-Hill Book Co., Inc., 1961.

3. Drayer, D E. and Timmerhaus, K. D.: An Experimental Investigation of the Individual Boiling and Condensing Heat-Transfer Coefficients for Hydrogen. Advances in Cryogenic Engineering, vol. 7, Proceedings of the 1961 Cryogenic Engineering Conference. pp. 401-411, Plenum Press, 1962.

4. Roder, Hans M., and Goodwin, Robert D.: Extended Tables of Provisional Thermodynamic Functions for Para Hydrogen. Rep. 7220, NBS, Jan. 3, 1962.

5. Scott, Russell B.: Cryogenic Engineering. D. Van Nostrand Co., Inc., 1959.

TABLE I. - SUMMARY OF EXPERIMENTAL RESULTS AND HEAT TRANSFER ANALYSIS

Test number	Initial percent filling	Pressure rise rate, psi/min	(Liquid) $\frac{\Delta T_{bulk}}{\Delta T_{sat}}$	(Vapor) ΔT_{max}, ^{o}R	q/A_1 average, $\frac{Btu}{hr\text{-}ft^2}$	q/A_1 wetted area, $\frac{Btu}{hr\text{-}ft^2}$	q/A_1 dry area, $\frac{Btu}{hr\text{-}ft^2}$
			Uniform heating				
1	34.6	3.5	0.55	110	17.5	20.0	15.7
2	51.4	3.6	.46	1 [illegible]	18.2	20.0	16.4
3	34.9	11.3	.62	212	59.9	80.3	45.8
4	48.9	13.5	.47	200	65.0	80.7	48.9
5	76.5	17.0	.32	159	72.6	80.5	54.1
6	36.8	19.3	.61	258	105.4	148.0	74.5
7	50.7	23.6	.47	245	111.6	142.7	78.4
8	77.2	30.3	.31	182	128.6	141.9	97.7
			Lower heating				
9	29.3	5.9	0.99	85	39.5	78.5	16.3
10	49.0	4.9	.99	109	44.6	81.7	5.1
11	73.5	3.6	.97	73	42.6	59.5	2.9
12	31.0	11.0	.95	87	73.3	146.6	27.3
13	47.8	8.6	.96	90	75.2	144.9	3.0
14	74.0	6.3	.92	54	75.7	105.4	3.5
			Upper heating				
15	36.5	4.6	0.10	81	15.5	1.5	25.2
16	50.5	5.8	.07	85	17.1	2.2	32.2
17	80.4	8.8	.05	99	19.6	13.8	34.0
18	34.3	8.2	.11	118	24.2	2.8	38.2
19	51.2	11.2	.06	123	27.6	4.6	51.7
20	47.7	18.5	.05	153	38.2	3.5	71.0
21	77.0	30.3	.04	158	53.6	42.6	77.8

TABLE 2. - RESULTS OF ENERGY DISTRIBUTION ANALYSIS

Test number	Average percent filling	Energy input to liquid wetted walls as percent of total	Q_{liquid}	Q_{vapor}	Q_{evap}	Q_{bulk}	Q_{layer}
			As percent of total energy input				
			Uniform heating				
1	35.8	46.4	77.4	8.8	13.8	32.5	44.9
2	52.9	57.2	82.9	6.7	10.3	51.7	31.2
3	36.7	54.9	76.1	18.1	5.8	39.1	37.0
4	50.4	62.7	79.3	15.4	5.2	58.4	20.9
5	78.2	77.5	91.0	7.7	1.2	64.6	26.4
6	38.4	59.2	74.5	22.0	3.6	47.8	26.7
7	52.2	66.0	77.4	18.7	3.9	65.5	11.9
8	78.7	77.1	90.8	8.7	0.6	63.8	26.9
			Lower heating				
10	52.8	94.4	85.4	3.5	11.1	82.6	2.8
11	79.4	98.2	97.1	0.9	2.1	95.6	1.5
13	50.9	98.1	84.7	3.6	11.8	80.9	3.8
14	79.9	98.8	96.9	0.9	2.3	96.9	----
			Upper heating				
15	36.9	4.1	70.9	9.7	19.4	5.6	65.3
16	50.7	6.6	70.8	8.4	20.8	6.2	64.6
18	34.6	4.5	67.6	14.6	17.8	8.0	59.6
19	51.2	8.6	66.3	12.4	21.4	5.4	60.9
20	47.7	4.4	59.3	18.9	21.8	4.8	54.5

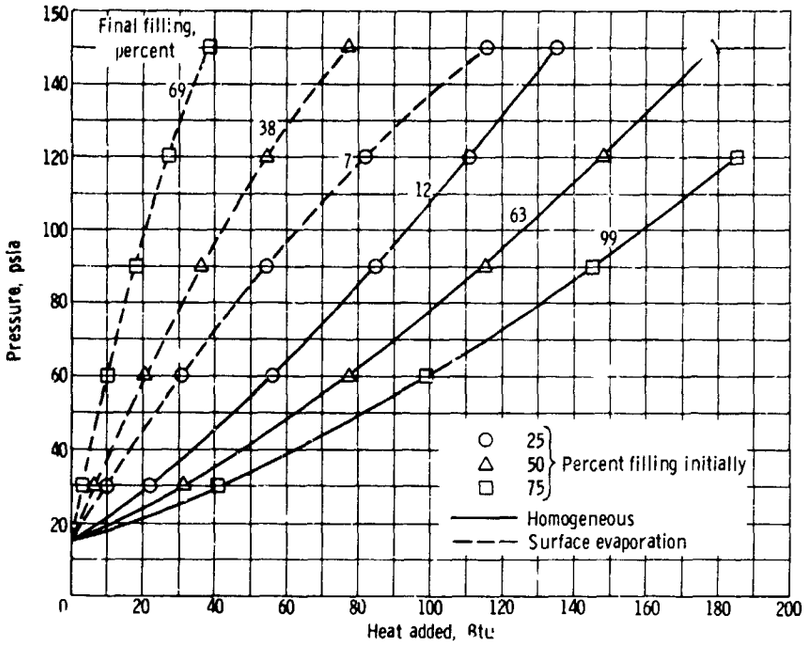

Figure 1. - Tank pressure as function of heat added for two-energy distribution models; 1-cubic-foot tank.

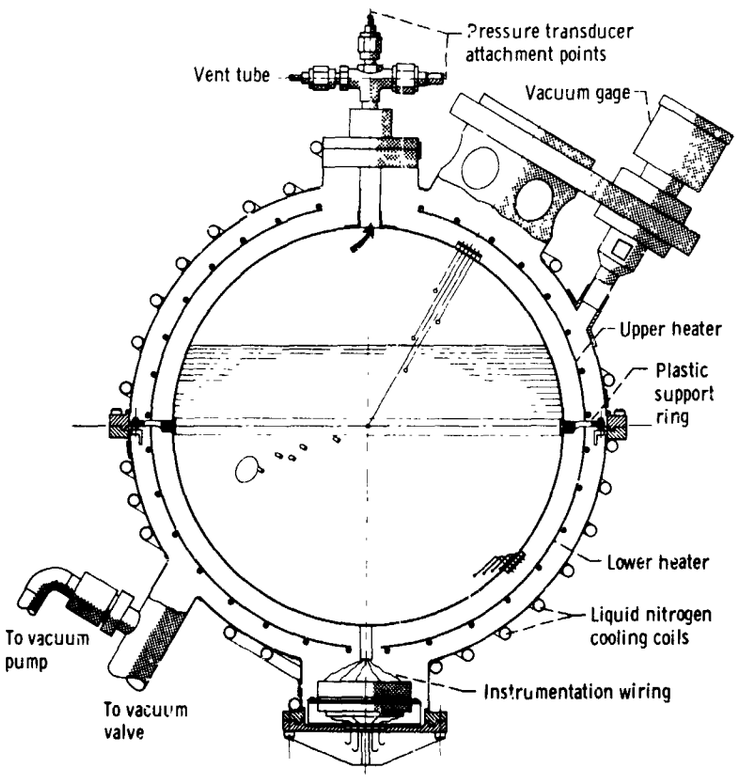

Figure 2. - Schematic drawing of liquid hydrogen experiment.

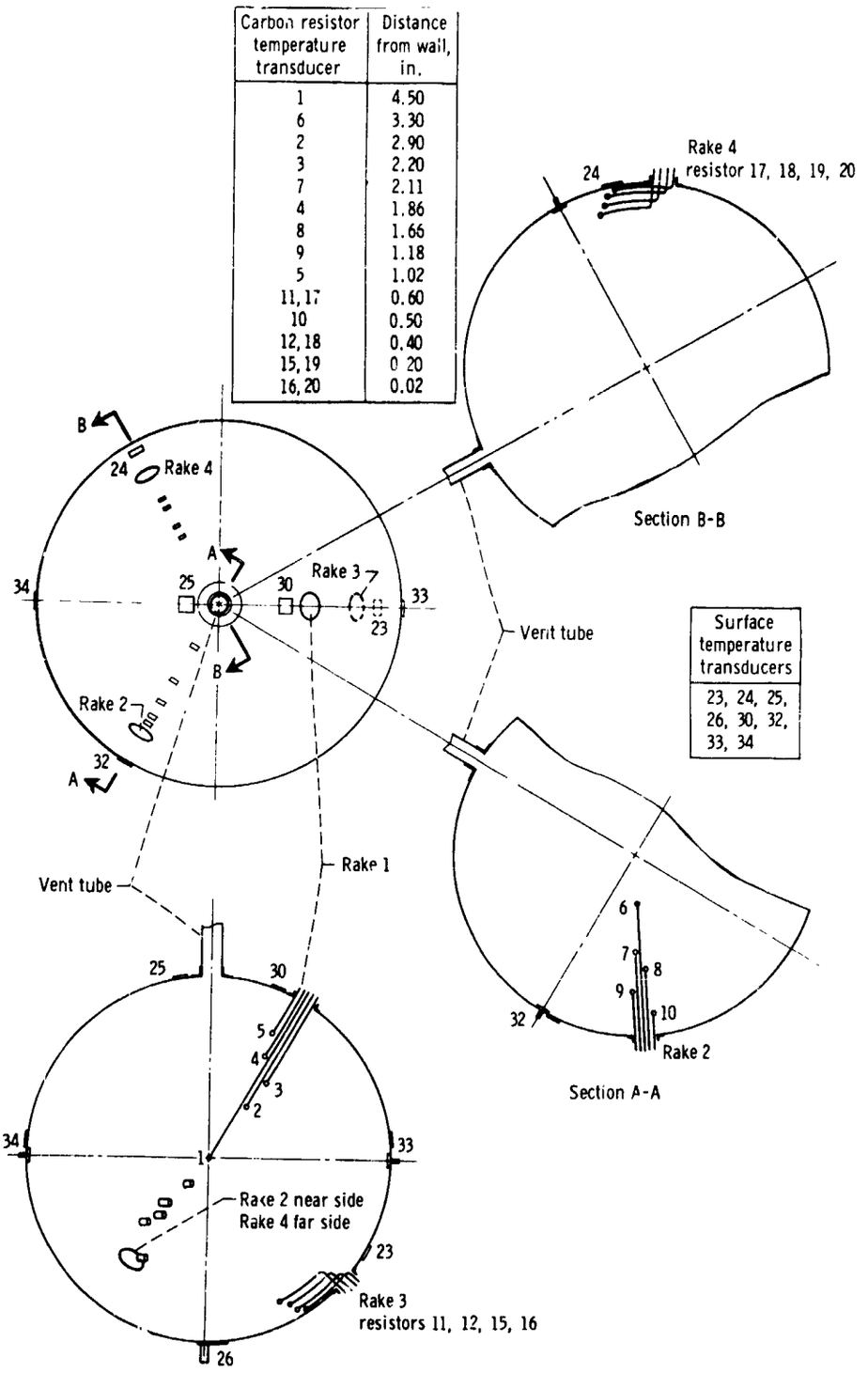

Figure 3. - Inner sphere temperature transducer locations.

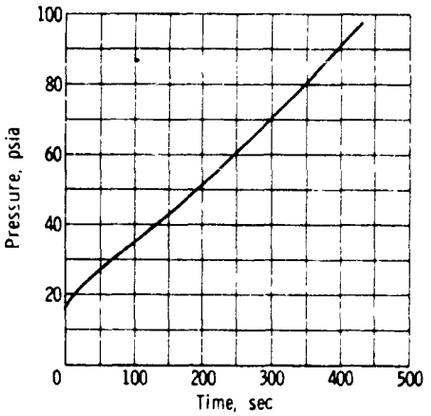

(a) Total pressure as function of time.

Figure 4. - Test number three.

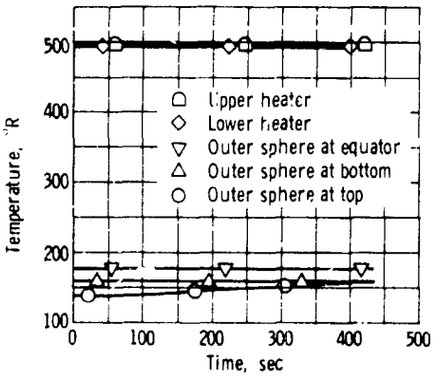

(b) Outer sphere and heater temperature as function of time

Figure 4. - Continued

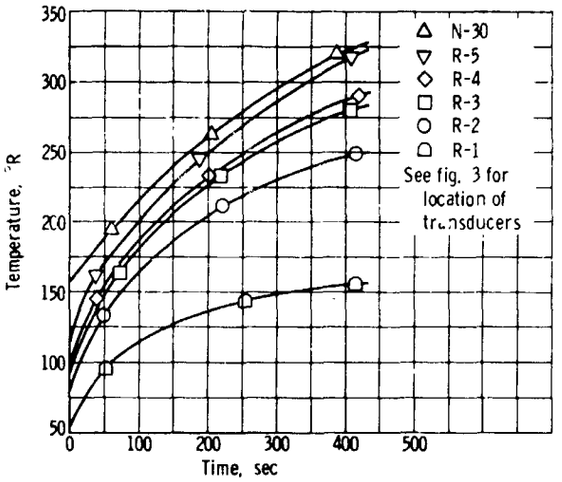

(c) Upper inner sphere temperature as function of time.

Figure 4. - Continued.

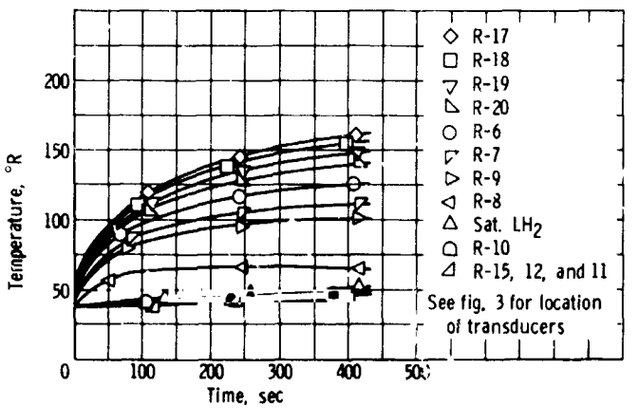

(d) Lower inner sphere temperature as function of time.

Figure 4. - Concluded.

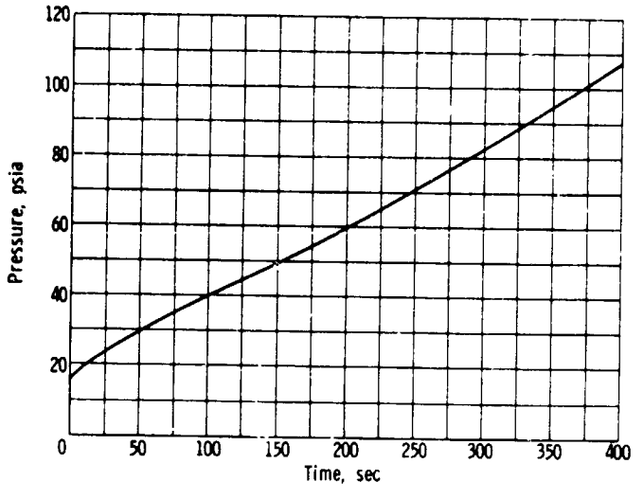

(a) Total pressure as function of time.

Figure 5. - Test number four.

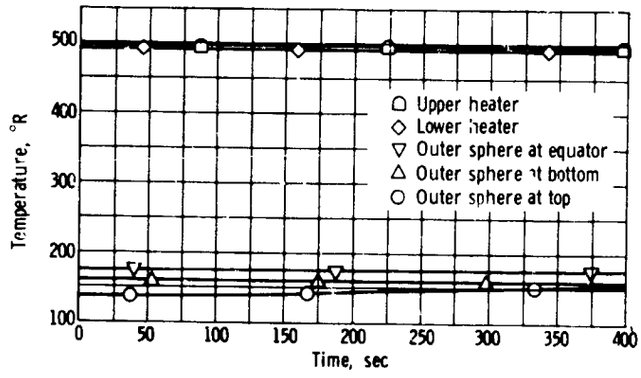

(b) Outer sphere and heater temperature as function of time.

Figure 5. - Continued.

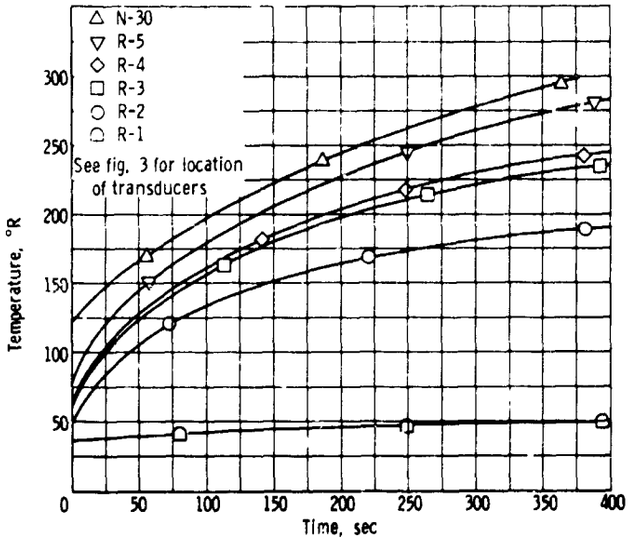

(c) Upper inner sphere temperature as function of time.

Figure 5. - Continued.

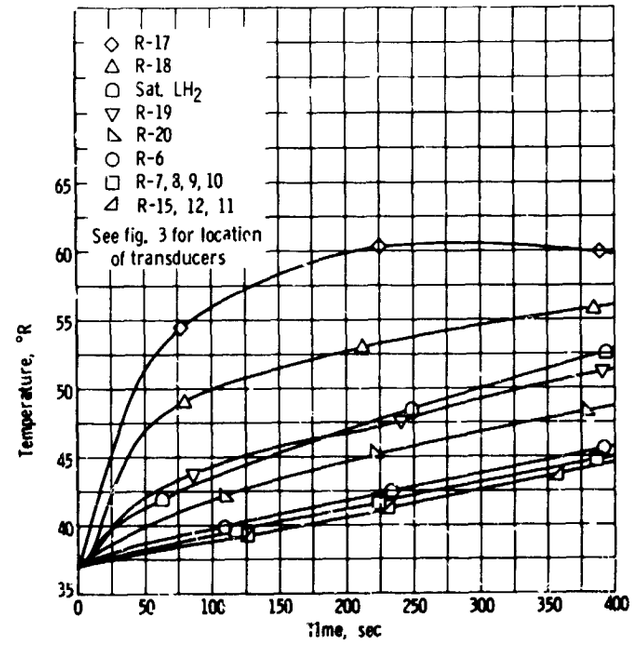

(d) Lower inner sphere temperature as function of time.

Figure 5. - Concluded.

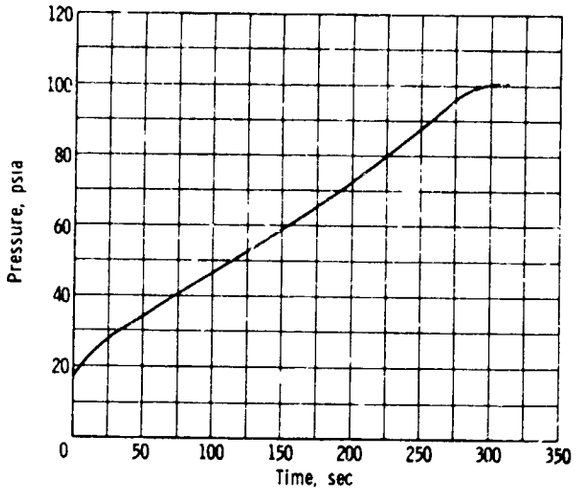

(a) Total pressure as function of time.

Figure 6. - Test number five.

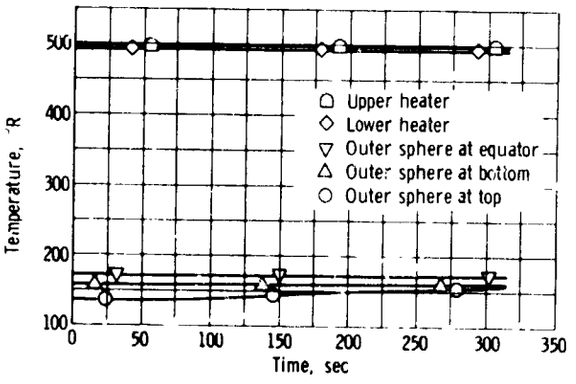

(b) Outer sphere and heater temperature as function of time.

Figure 6. - Continued.

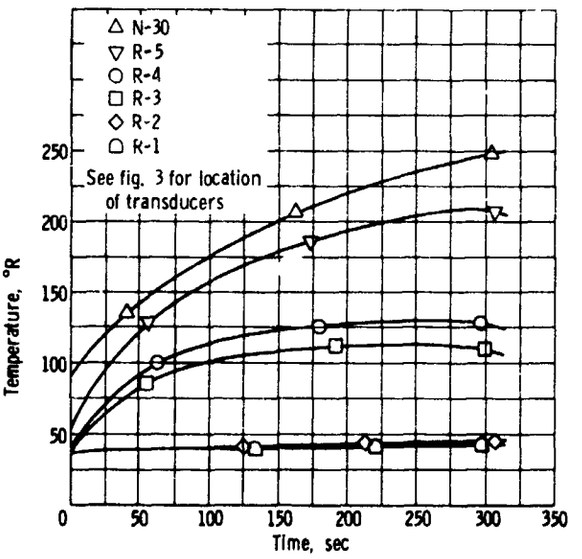

(c) Upper inner sphere temperature as function of time.

Figure 6. - Continued.

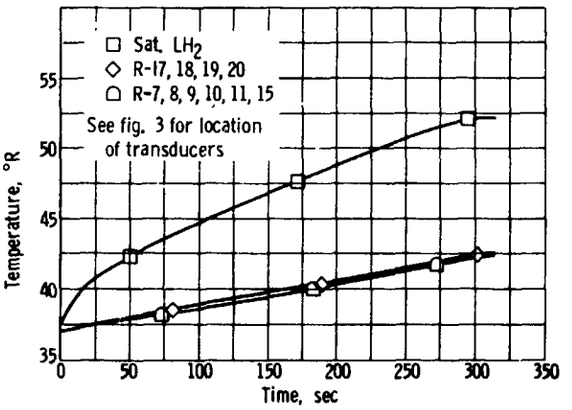

(d) Lower inner sphere temperature as function of time.

Figure 6. - Concluded.

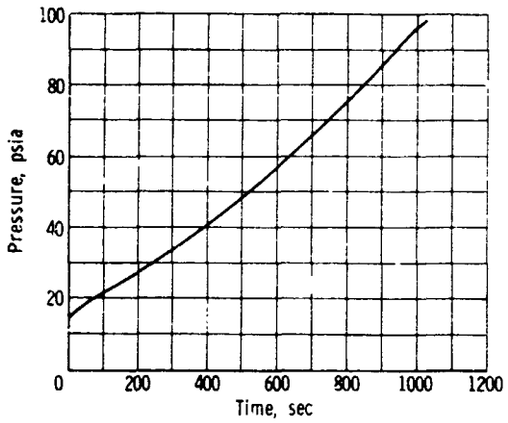

(a) Total pressure as function of time.

Figure 7. - Test number ten.

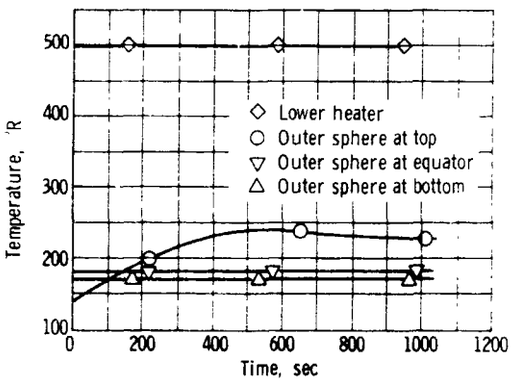

(b) Outer sphere and heater temperature as function of time.

Figure 7. - Continued.

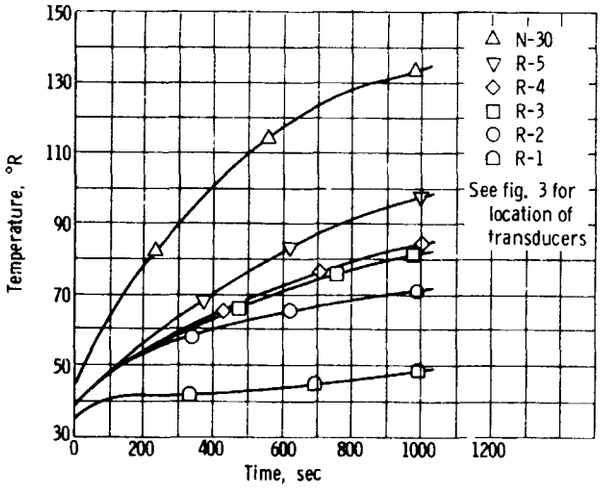

(c) Upper inner sphere temperature as function of time.

Figure 7. - Continued.

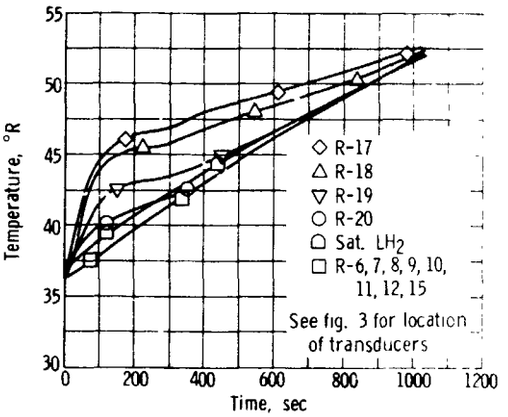

(d) Lower inner sphere temperature as function of time.

Figure 7. - Concluded.

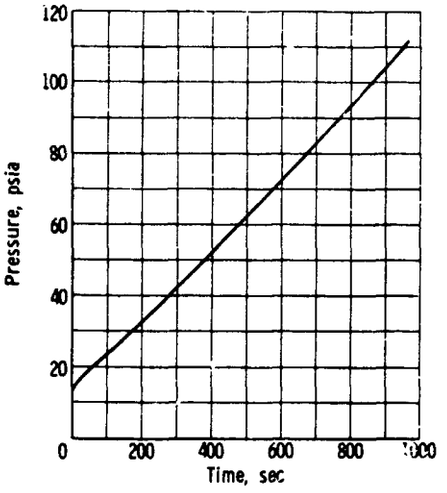

(a) Total pressure as function of time.

Figure 8. - Test number sixteen.

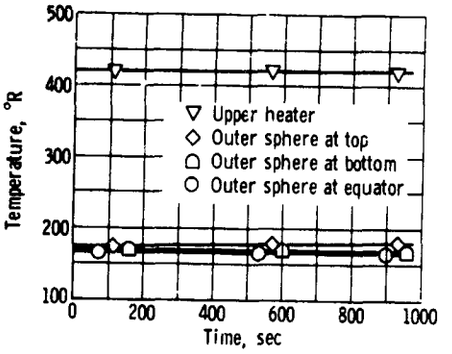

(b) Outer sphere and heater temperature as function of time.

Figure 8. - Continued.

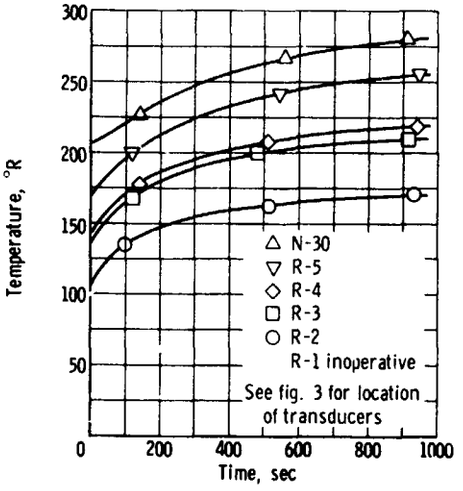

(c) Upper inner sphere temperature as function of time.

Figure 8. - Continued.

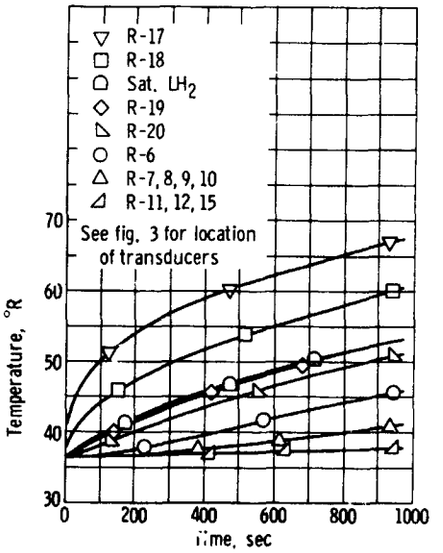

(d) Lower inner sphere temperature as function of time.

Figure 8. - Concluded.

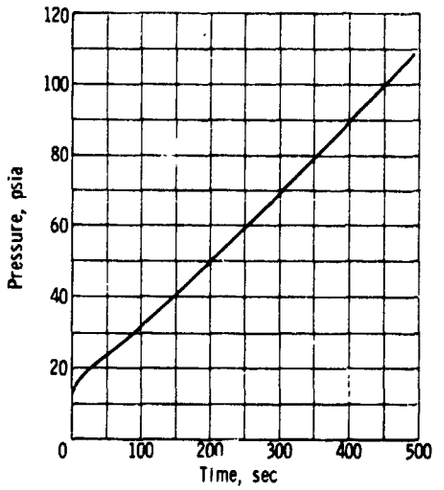

(a) Total pressure as function of time.

Figure 9. - Test number nineteen.

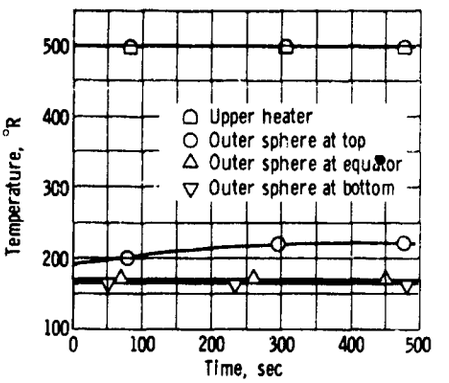

(b) Outer sphere and heater temperature as function of time.

Figure 9. - Continued.

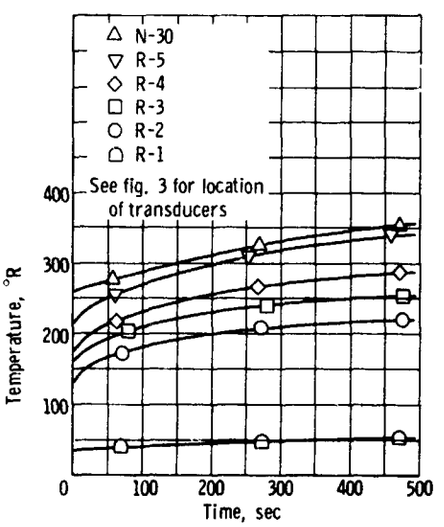

(c) Upper inner sphere temperature as function of time.

Figure 9. - Continued.

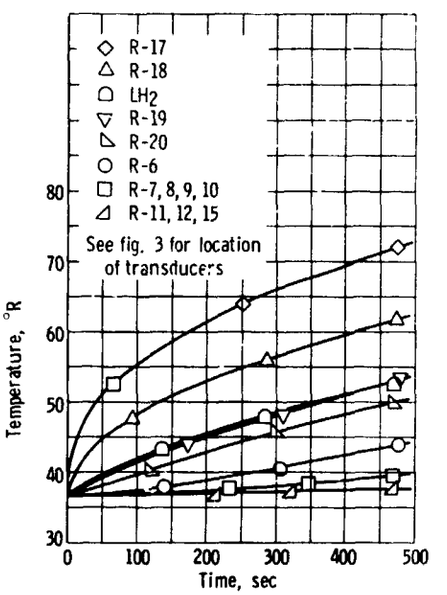

(d) Lower inner sphere temperature as function of time.

Figure 9. - Concluded.

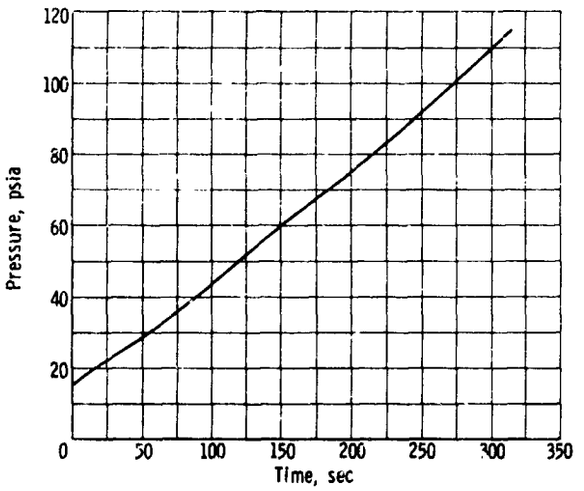

(a) Total pressure as function of time.

Figure 10. - Test number twenty.

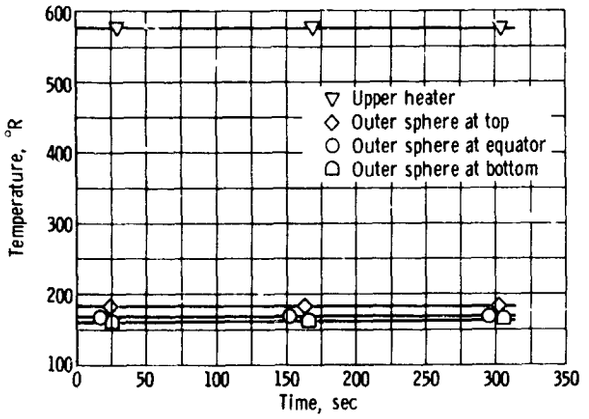

(b) Outer sphere and heater temperature as function of time.

Figure 10. - Continued.

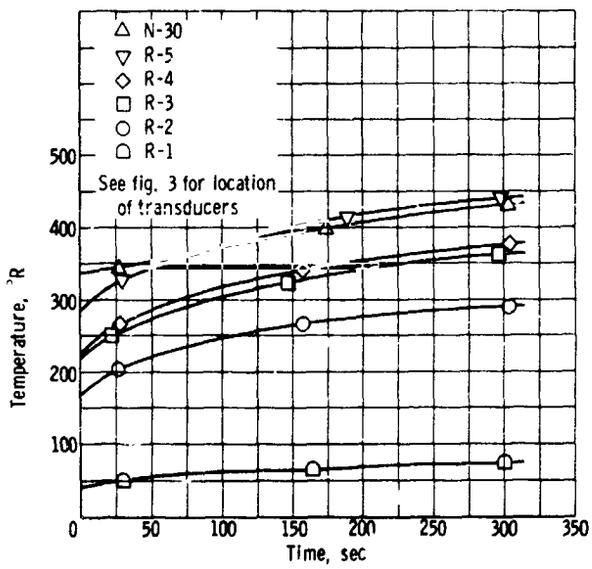

(c) Upper inner sphere temperature as function of time.

Figure 10. - Continued.

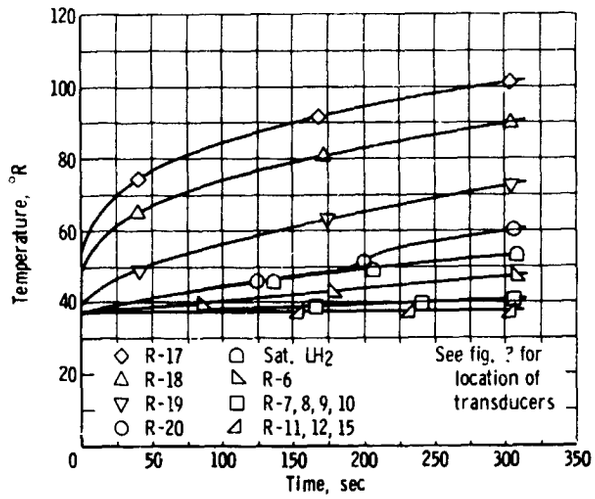

(d) Lower inner sphere temperature as function of time.

Figure 10. - Concluded.

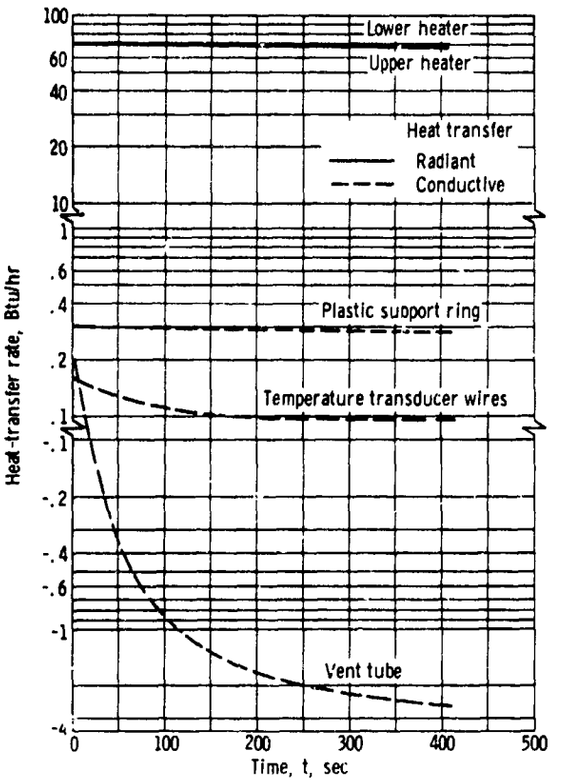

Figure 11. - Rate of heat input as function of time for each heat source for typical quiescent test.

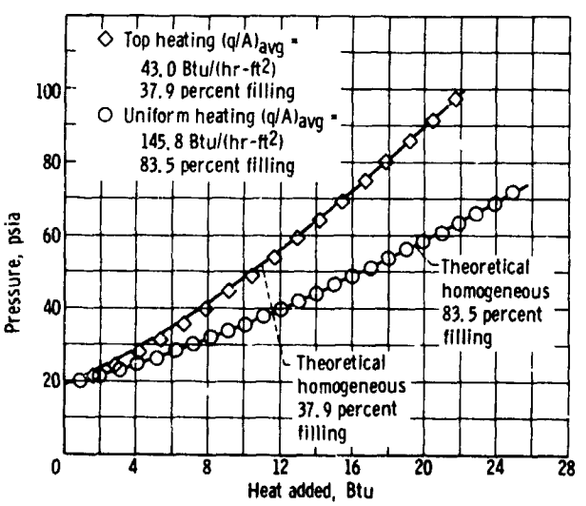

Figure 12. - Pressure as function of total heat added for two homogeneous tests.

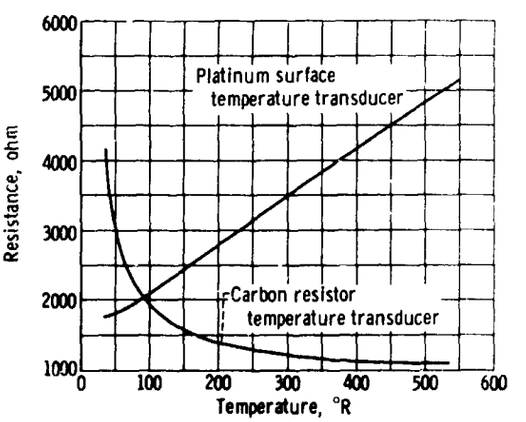

Figure 13. - Resistance as function of temperature for typical inner sphere temperature transducers.

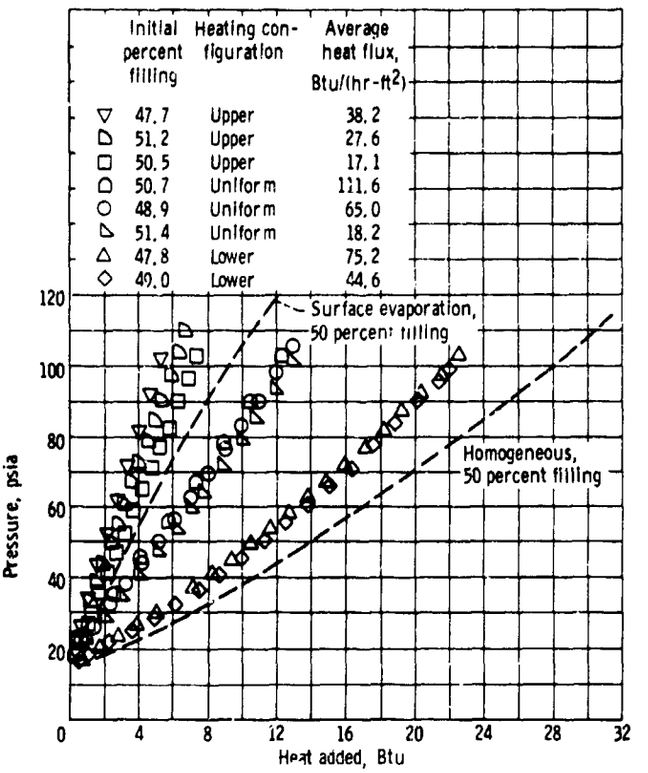

(a) Effect of heat transfer rate and distribution.

Figure 14. - Pressure as function of total heat added for quiescent tests.

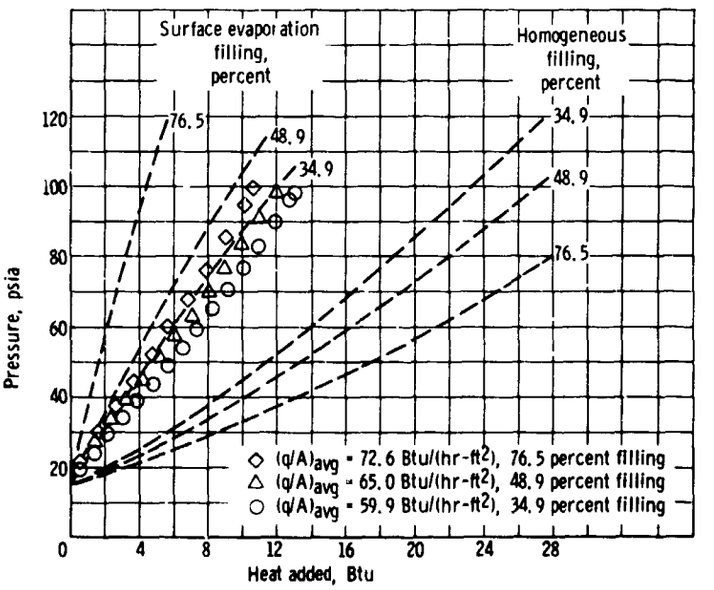

(b) Effect of percent filling.

Figure 14. - Concluded.

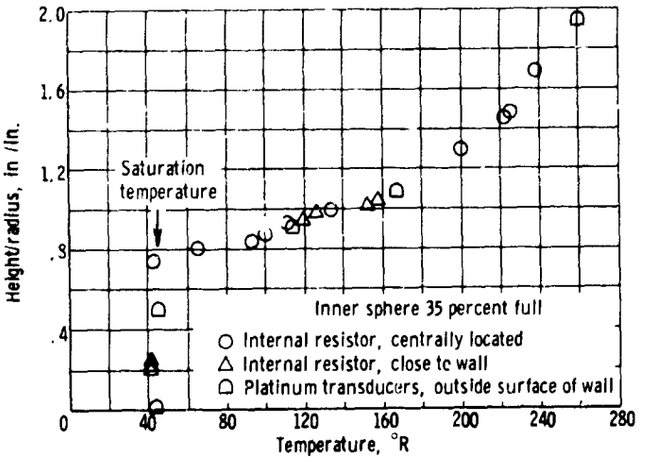

Figure 15. - Inner sphere temperature as function of position for typical quiescent test.

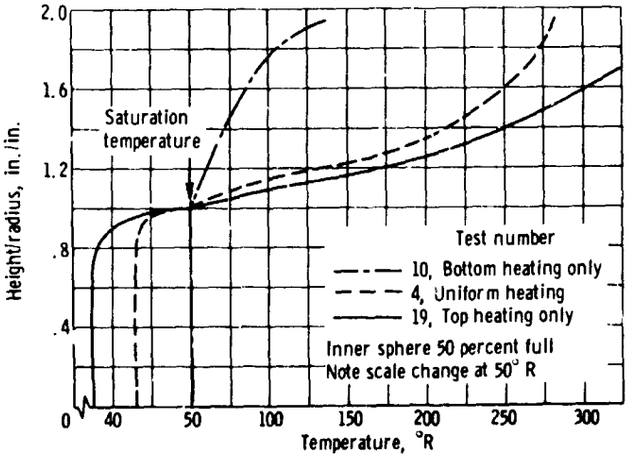

Figure 16. - Inner sphere temperature as function of position for three heating configurations.

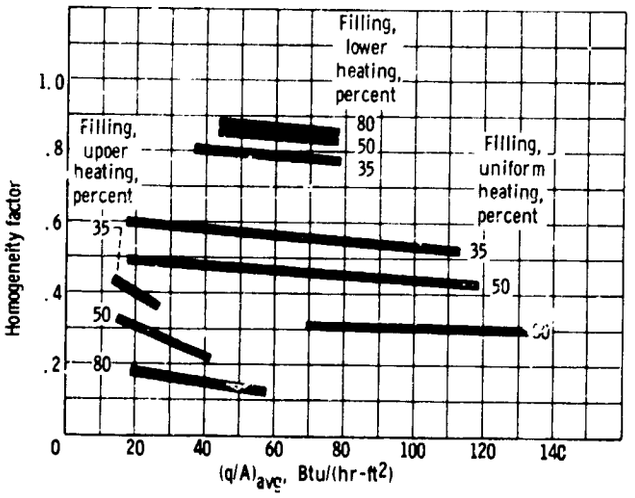

Figure 17. - Homogeneity factor as function of average heat transfer rate.

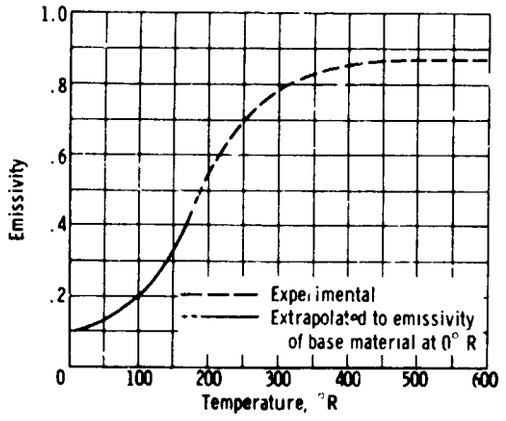

Figure 18. - Inner sphere and heater emissivity as function of temperature.

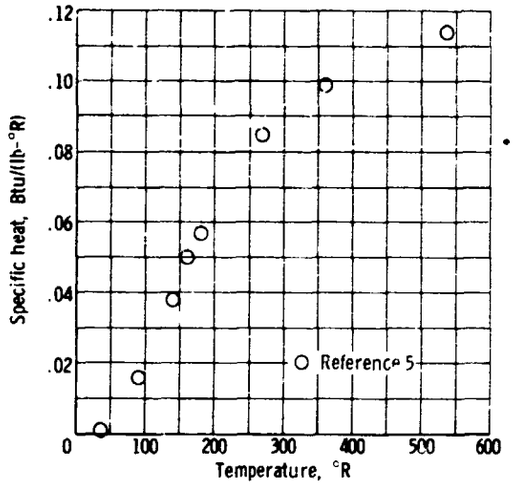

Figure 19 - Stainless steel specific heat as function of temperature.

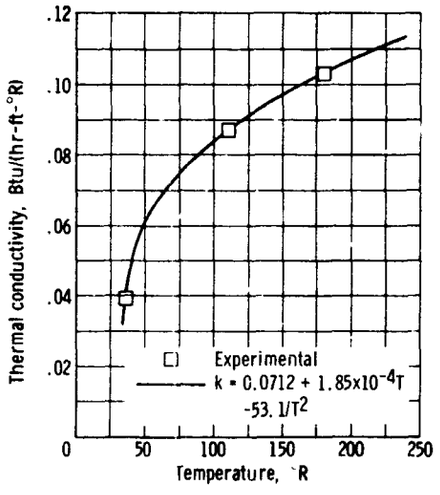

Figure 20. - Plastic support ring thermal conductivity as function of temperature.

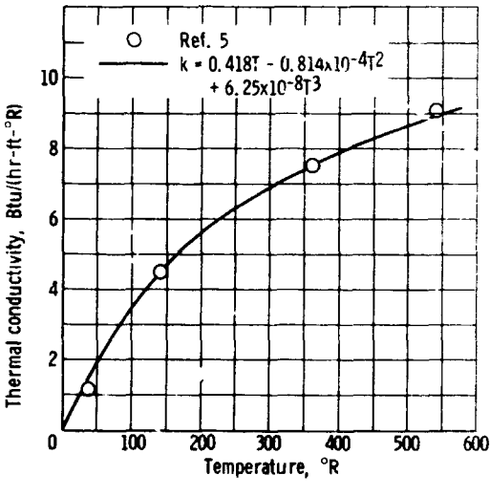

Figure 21. - Stainless steel thermal conductivity as function of temperature.